Published in final edited form as:
J Microsc. 2008 December ; 232(3): 432–441. doi:10.1111/j.1365-2818.2008.02138.x.

Ex vivo characterization of human atherosclerotic iliac plaque components using cryo-imaging

M.S. Nguyen[*], **O. Salvado**[†], **D. Roy**[‡], **G. Steyer**[‡], **M.E. Stone**[‡], **R.D. Hoffman**[§], and **D.L. Wilson**[‡,¶]

[*]School of Medicine, Case Western Reserve University, Cleveland, OH44106, U.S.A.

[†]CSIRO–The Australian e-Health Research Centre, Brisbane, QLD 4000, Australia

[‡]Department of Biomedical Engineering, Case Western Reserve University, Cleveland, OH44106, U.S.A.

[§]Department of Pathology, University Hospitals of Cleveland, Cleveland, OH 44106, U.S.A.

[¶]Department of Radiology, University Hospitals of Cleveland Cleveland OH44106, U.S.A.

Abstract

We characterized atherosclerotic plaque components with a novel cryo-imaging system *in lieu* of standard histological methods commonly used for imaging validation and research endpoints. We aim to accurately identify plaque tissue types from fresh cadaver specimens rapidly (less than 5 h) in three dimensions for large specimens (up to 4 cm vessel segments). A single-blind validation study was designed to determine sensitivity, specificity and inter-rater agreement (Fleiss' Kappa) of cryo-imaging tissue types with histology as the gold standard. Six naïve human raters identified 344 tissue type samples in 36 cryo-image sets after being trained. Tissue type sensitivities are as follows: greater than 90% for adventitia, media-related, smooth muscle cell ingrowth, external elastic lamina, internal elastic lamina, fibrosis, dense calcification and haemorrhage; greater than 80% for lipid and light calcification; and greater than 50% for cholesterol clefts. Specificities were greater than 95% for all tissue types. The results demonstrate convincingly that cryo-imaging can be used to accurately identify most tissue types. If the cryo-imaging data are entered into visualization software, three-dimensional renderings of the plaque can be generated to visualize and quantify plaque components.

Keywords

atherosclerosis; cryo-imaging; CT; histology; MR

Introduction

Atherosclerotic plaque composition is the primary determinant in whether a plaque is likely to rupture (Ross, 1999; Libby *et al.*, 2002). Multiple *in vivo* 3D imaging modalities have been used to characterize plaque composition: computerized tomography (CT) (de Weert *et al.*, 2006), magnetic resonance imaging (MRI) (Larose *et al.*, 2005; Yuan *et al.*, 2006) and intravascular ultrasound (IVUS) (Granada *et al.*, 2007). These modalities allow identification

Correspondence to: D.L. Wilson. Tel: 216-368-4099; fax: 216-368-4969; e-mail: E-mail: david.wilson@case.edu.

Disclosures:
Dr. Wilson founded BioIn Vision, Inc. to commercialize cryo-imaging technology.

of lipid (Larose *et al.*, 2005; de Weert *et al.*, 2006; Yuan *et al.*, 2006; Granada *et al.*, 2007), fibrous cap (Larose *et al.*, 2005; de Weert *et al.*, 2006; Yuan *et al.*, 2006; Granada *et al.*, 2007), calcification (Larose *et al.*, 2005; de Weert *et al.*, 2006; Yuan *et al.*, 2006; Granada *et al.*, 2007) and necrotic core areas which include haemorrhage (Yuan *et al.*, 2006; Granada *et al.*, 2007).

The gold standard to validate these modalities is histology which typically consists of obtaining consecutive rings (2–3 mm) of the vessel after imaging and processing them with common staining techniques (Larose *et al.*, 2005; de Weert *et al.*, 2006; Yuan *et al.*, 2006; Granada *et al.*, 2007). There are several major drawbacks to using 2D histology to validate these 3D modalities. During histology processing, the tissue shrinks and deforms from its natural shape and may develop artefacts such as folds and tears. Some tissue types such as the lipid core may wash out whereas other tissue types may not be identified without special steps. Accurately registering the imaging slice location to the histology is also error prone. For example, a recent literature review found that comparing the correlation between carotid plaque imaging and histology with several imaging modalities was highly variable and unreliable because of lack of imaging–histological standards (Lovett *et al.*, 2005). In summary, histology is not the ideal validation method for *in vivo* 3D imaging modalities.

We are introducing cryo-imaging as a new and alternative validation method for *in vivo* 3D imaging studies (Fig. 1). Cryo-imaging utilizes a large-specimen cryo-microtome with a mounted episcopic microscope and charge-coupled device (CCD) camera to obtain block face images of embedded frozen tissue samples (Salvado *et al.*, 2006a,b).

Unlike histology, cryo-imaging preserves *in vivo* plaque architecture and components and is therefore a better validation method for many 3D imaging modalities (IVUS, MRI and CT). Furthermore, cryo-imaging can be used to identify many more tissue types and with greater granularity than the typical lipid core, fibrous cap and calcification seen with the standard imaging modalities. Fifteen tissue types are described in this study.

Cryo-imaging has many other possible applications. The cryo-imaging data can be entered into visualization software to generate accurate 3D renderings for plaque visualization and quantification. For example, the vasa vasorum can be studied in this manner to help determine if plaque angiogenic signals induce neovascularization (Fleiner *et al.*, 2004). Cryo-imaging can be used with immunostains to delineate further information about plaque components.

To measure cryo-imaging interpretation reproducibility, we performed a single blind study with histology as the gold standard. We first identified tissue types observable in cryo-images and then established a set of rules that can be used to identify them. Using a group of six na¨ive human raters who were trained to evaluate cryo-images, we determined sensitivity, specificity and inter-rater agreement (Fleiss' Kappa) for each tissue type. For demonstration purposes, 3D renderings of a vessel specimen are shown.

Methods

Specimen

Bilateral common iliac arteries from five men and four women cadavers with an age range of 42 to 86 years old were obtained (65.0 ± 18.0 years old). Autopsies were performed within 42 h after death (20.5 ± 10.7 h) and the vessel specimens were stored in a sealed container at 4° C after removal from body. Specimens included examples with American Heart Association's lesion types I–VI (Stary *et al*, 1994, 1995). We obtained approval from the Case Institutional Review Board to work with the specimens in compliance with federal, state and local laws.

Cryo-imaging

Within 3 h after removal from body, the samples were retrieved, immersed in 0.9% saline solution for 1 h, washed gently with tap water to remove blood clumps, cut into 2.5 cm segments and embedded in cryo-histological medium gel [Tissue-Tek optimum cutting temperature (OCT) Compound, Sakura Finetech USA, Inc., Torrance, CA, USA]. The embedded vessels were then stored at −80°C until cutting.

Prior to cutting, the vessel blocks were removed from the −80°C freezer and equilibrated to the cutting temperature of −20°C by placing them in the cryo-imaging system for 30 min. The blocks were then mounted onto the stage of a cryo-microtome (8250 Large Section Cryostat, Vibratome, St. Louis, MO, U.S.A.). The microtome stage allows for samples up to 250 × 110 × 40 mm. Slice thickness is manually adjustable from 4 to 40 μm.

After mounting, serial 40-μm sections were trimmed from the blocks until the entire circumference of the vessel could be clearly seen and a flat block face free of imperfections was visible. A digital colour CCD camera (Retiga Exi, QImaging, Surrey, BC, Canada) attached to a stereo microscope (SZX12, Olympus, Tokyo, Japan) was used to capture images. For blood vessel imaging, a 0.3 × objective and 7.5 × magnification was typically used giving a pixel resolution of 18.0 × 18.0 μm and a field of view of 24.48 × 18.65 mm. A bright light illuminator (DCRIII Plus, Schott, NY, USA) was used for bright-field imaging and blue light excitation (460–490 nm) and green flourescent protein (GFP) emission (510 nm) filters were used for fluorescence imaging. Typical exposure time was about 10 ms for bright-field imaging and 3000 ms for fluorescence imaging. Both bright-field and fluorescence images were obtained in colour using the same red, green, blue (RGB) wheel (RGB-Slider, QImaging). White balance and exposure time were calibrated using a white sheet of paper using manufacturer software auto-calibration functions. Bright-field images were divided by the white image to correct for the uneven illumination.

For each block face, one set of bright-field and fluorescence images was taken (Fig. 2a and b) at the same position and magnification. Afterwards, a 2-mm-thick slice was made to retrieve a vessel ring sample for histology. This process was repeated until the whole vessel was sliced.

To reduce sub-surface illumination, a high-pass filter weighted by the colour saturation was applied to the bright-field image to generate the contrast-enhanced bright-field image (Fig. 2c). To obtain high-contrast tissue differentiation consistent across patients using information from the otherwise low-contrast fluorescence images (Fig. 2b), we generated a specific pseudo-colour image (Fig. 2d). We observed that the green auto-fluorescence was absorbed mostly by haemoglobin which exhibited auto-fluorescence in the red channel. We therefore created a new channel dividing the green by the red channel of the fluorescence image. The result was re-scaled between 0 and 1 and used as the hue plane of a new pseudo-colour image. In order to relate this new contrast to the RGB image, we used the saturation and value planes from the contrast-enhanced bright-field image (Fig. 2c). The resulting new pseudo-colour image (Fig. 2d) allows tissues to be easily identified based on their haemoglobin content in addition to their auto-fluorescence properties.

Histology

Vessel ring samples that showed significant lipid areas underwent frozen section Oil Red O staining. Other ring samples had standard histological preparations: haematoxylin and eosin, Elastic van Gieson and Mallory's trichrome. For the standard histological preparations, samples were fixed overnight in 10% formalin solution and then decalcified in Surgipath Decalcifier II solution for 2 h. The stains were performed by the university's histology service using routine protocols.

Tissue types

After meticulously comparing the bright-field, fluorescence and pseudo-colour cryo-images with each other and to the corresponding histology, a set of robust rules was created to identify tissue types on cryo-images (Table 1 and Fig. 3). Tissue type colours in bright-field and pseudo-colour cryo-images and fluorescence intensities were recorded. Pertinent histology characteristics were also noted. The rules were determined after careful examination by three experts, including a board-certified pathologist.

Validation study

To test the robustness of the rules, a single-blind validation study was performed with six naïve human raters, comprised of three undergraduate and three graduate students. The raters were first trained using a training guide that included a brief overview of atherosclerosis, the rule set (Table 1), examples of each tissue type (Fig. 3) and practice image sets. Each image set included matching bright-field, contrast-enhanced bright-field, fluorescence and pseudo-colour cryo-images arranged in quadrant form (Fig. 2). Arrows with numbered labels pointed to the tissue of interest for the rater to identify. The tissue types to be identified were carefully selected after confirmation with matching histology or unequivocal evidence on the cryo-images, such as the case with haemorrhage which is washed out by histology processing. For each image set, as many tissue types as possible were labelled. Because some tissue types were more common than others, the distribution of tissue type items was determined in large part by how often that tissue type occurred naturally among the specimens. The raters reviewed the guide for 5 h over 5 days. A short pre-assessment was given at the end of the fifth day to determine readiness and to provide familiarity with the format of the validation study.

In the training guide, image sets from four of the patients were included. The pre-assessment used image sets found in the training guide. The validation study used new images sets from all nine patients who had not been previously included in the training guide. The validation study was constructed using four image sets from each of the nine patients for a total of 36 image sets and 344 tissue type samples to identify. Of the four image sets from each patient, one was verified against Oil Red O stain, whereas the other three sets were verified using the other matching stains. Image sets from both right and left sides of the common iliac arteries for each patient was used. The validation study required approximately 15 h over 5 days to complete. The raters could refer to the training guide while doing the validation study because new images were used in the study.

Results

Fifteen tissue types were described by the experts using cryo-imaging (Table 1). Four of the tissue types (adventitia, media, external elastic lamina and internal elastic lamina) are part of the normal anatomy of a blood vessel and the rest are pathological. Examples of each tissue type are shown in Fig. 3. Bone and bone marrow were also seen, but they were not described in this study for reasons elaborated in the ‘Discussion’ section.

The results of the validation study showed that adventitia, media-related, smooth muscle cell ingrowth, external elastic lamina, internal elastic lamina, fibrosis, dense calcification and haemorrhage had sensitivities greater than 90%, lipid and light calcification had sensitivities greater than 80%, and cholesterol clefts had the worst performance with sensitivities above 50%.

Because of the ambiguous nature of distinguishing certain tissue types in this experimental setup, to be discussed in detail in the ‘Discussion’ section, the results of certain tissue types were evaluated both individually and combined. The tissue types that were combined were the

media and calcified media tissue types, the fluorescent and non-fluorescent fibrosis tissue types, and the diffuse, concentrated and highly concentrated haemorrhage tissue types, respectively.

The study results for all raters for all tissue types are shown in Table 2 in contingency table format. The histology ground truth results are shown as the horizontal categories and the rater results on the cryo-images are shown as the vertical categories. Perfect agreement would give all values in the diagonal and zeros everywhere else. When tissue types are misidentified, the table reveals other tissue types that are most commonly mistaken for a particular tissue type. It was noted that media and calcification in media; fluorescent and non-fluorescent fibrosis; and diffuse, concentrated and highly concentrated haemorrhage tissue types were most often mistaken with each other, respectively. A contingency table where these tissue type categories have been combined is shown in Table 3.

The sensitivity, specificity, and Fleiss' Kappa for each tissue type are shown in Fig. 4. Fleiss' Kappa is a statistical measure of inter-rater agreement when more than two raters are used. Minitab 14 statistical software (Minitab Inc., State College, PA, U.S.A.) was used to calculate Fleiss' Kappa. When Fleiss' Kappa is near unity, there is good agreement among the raters for that tissue type. Specificity was calculated to be greater than 95% for all tissue types (not shown). The high specificity is a result of having many possible tissue types for the raters to choose from, leading to disproportionate number of true negatives. Figure 4(b) shows media, fibrosis and haemorrhage combined categories have higher sensitivities and Fleiss' Kappa's and narrower 95% confidence intervals than individual categories (Fig. 4a).

The overall average sensitivities before and after combining ambiguous categories are 83.0 ± 3.6% and 89.1 ± 2.7%, respectively, and 83.9 ± 0.7% and 88.4 ± 0.8% for Fleiss' Kappa. If the results of the two raters who had the lowest averages are eliminated, the average sensitivities before and after combining categories improve to 85.0 ± 3.0% and 90.0 ± 2.0%, respectively, and 86.7 ± 0.9% and 91.0 ± 1.0% for Fleiss' Kappa. We note that these two persons had no prior experience in the critical evaluation of images.

Each rater scored at least 80% overall. The average performance for all raters before and after combining categories is 85.5 ± 1.5% and 89.8 ± 1.3%, with the highest scores being 89.2% and 92.7%, respectively.

Discussion

Results can be divided into tissue types where the sensitivities and inter-rater agreements were high (adventitia, smooth muscle cell ingrowth, external elastic lamina, internal elastic lamina, lipid), slightly ambiguous (media, fibrosis and haemorrhage categories) and poor (cholesterol clefts). The results of the ambiguous tissue types were combined during analysis because it was determined that the ambiguities were probably due to experimental setup. These results do not limit validation of *in vivo* 3D imaging modalities because these modalities cannot distinguish between these tissue sub-types, e.g. MRI cannot distinguish fibrosis tissue types.

The ambiguity of the media and haemorrhage tissue types most likely stemmed from the question format. Calcified media were often confused with media because the rater may not have realized that the arrow was pointing specifically to the calcified media and not the surrounding media and vice versa. Similarly, haemorrhage tissue types were frequently confused because they often segue into each other and occur in small quantities; the raters had some difficulty deciding which haemorrhage type that the arrow was pointing to. These tissue types are in fact fairly easy to identify once the rater has been trained. To investigate this further, three of the raters later reviewed together seven questions from the validation study related to

these tissue types where half or fewer of all raters responded correctly. On five questions, raters were able to reach unanimous consensus. The other two questions had majority agreement.

Another ambiguity caused by the experimental setup was fluorescent versus non-fluorescent fibrosis. Fibrosis fluorescence is really a continuous spectrum from low to high values without clear discrete boundaries. For example, an area of fibrosis may be mostly non-fluorescent with small streaks of fluorescent fibrosis. Furthermore, the raters were not given a fluorescence intensity cutoff value to separate fluorescent from non-fluorescent fibrosis. Thus, distinguishing fibrosis into only two types was entirely subjective. This gave a valid rationale for combining these two tissue types. It is interesting to note that the fluorescence property is seen only in the cryo-images and not in the histology stains we used. Under histology, both fluorescent and non-fluorescent fibrosis appear as dense mature collagen. Interestingly, collagen found in bone has been demonstrated to have fluorescence properties (Prentice, 1967). With more than 10 known collagen types in the human body, an area of further investigation is to determine which types have fluorescent properties.

In the specimens we examined, examples of both intimal and medial arterial calcifications were observed. Intimal calcification is associated with atherosclerosis whereas medial calcification is known as Mönckeberg's sclerosis and is not a known risk factor or predictor of atherosclerosis (Doherty *et al.*, 2004). The rationale for including medial calcification as a tissue type is because it is identifiable with cryo-imaging and it can occur concurrently with atherosclerosis. Although both light and dense medial calcifications were observed, a single category was used because it was predominately dense (Fig. 3u). Although the literature does not differentiate intimal calcification into subtypes, we used the light and dense calcification naming scheme because clear differences could be observed on cryo-images and histology and both subtypes were found frequently (Fig. 3i–l). The sensitivities and Fleiss' Kappa's are 80.4 ± 7.4% and 82.1 ± 2.2% for light calcification and 93.8 ± 9.8% and 84.6 ± 2.2% for dense calcification. Table 2 shows that light calcification was often misidentified as dense calcification whereas the converse was not true. Like the different types of haemorrhage, light and dense calcification often segued into each other. Dense calcification may represent older or more compacted calcification compared to light calcification. Whether the 3D imaging modalities are able to detect the differences remains to be shown. The clinical significance in being able to classify different types of calcification is not clear either. Interestingly, intimal and medial calcifications show differences in fluorescence. Light and dense intimal calcifications and light medial calcification exhibit very strong fluorescence whereas dense medial calcification has little fluorescence (Fig. 3j and v). Another form of calcification that was observed in the plaque is bone. Both bone and bone marrow were observed on some histology slides, but they were not included in the tissue type characteristics table because of their rarity and that their occurrence in very small quantities made it very difficult to ascertain their cryo-imaging properties accurately.

Several reasons explain the poor rater performance with cholesterol clefts. First, there were only five questions pertaining to cholesterol clefts, as it did not occur often compared to other tissue types in our database. If a rater missed just one question, performance would already be impacted significantly. Second, cholesterol clefts occurred in small areas and were easy to overlook. Finally, the blue-green colour of cholesterol clefts on pseudo-colour cryo-images made it difficult to distinguish them from the green colour of diffuse haemorrhage. The algorithm used to generate pseudo-colour cryo-images is being evaluated to make cholesterol clefts more apparent. If cholesterol clefts were characterized by an unambiguous colour, then sensitivity and inter-rater agreement would increase substantially. Because cholesterol clefts are often found in quantities too small to be detected with current 3D *in vivo* imaging modalities, the relatively low sensitivity to cholesterol clefts is not a major deterrent to using cryo-imaging as a validation tool for plaque imaging.

The external and internal elastic laminae are tissue types that are not discernable in the bright-field or pseudo-colour cryo-images, but easily seen on the fluorescence cryo-image (Fig. 3u–w). The Elastic van Gieson stain which stains elastin fibres black was used to histologically verify the presence of the laminae (Fig. 3x). Because the laminae are composed mostly of elastin fibres, this suggests that elastin fibres also exhibit very strong fluorescence.

Haemorrhage tissue types were washed away by processing and were not seen on histology. Before embedding the vessels into OCT, they were gently washed to remove any blood clumps from the lumen. Therefore, the source of the haemorrhage seen on the cryo-images is not from blood sticking to the vessel walls but probably from plaque neovascularization or leaking vasa vasorum. In a side experiment, imaged 2-mm vessel rings with visible haemorrhage areas were thawed in tap water overnight at normal room temperature, re-embedded in OCT and refrozen. Upon re-imaging, the haemorrhage areas were no longer seen. We concluded that the water caused the haemorrhage areas to break up and diffuse away from the vessel. Interestingly, this procedure caused other areas of the vessel including the adventitia and media to lose their red hue, suggesting that the redness in these areas came from remnant blood.

In another side experiment, we investigated how vessel appearance changes if there is a delay in embedding and storing the specimens in the −80°C freezer. We simulated this by cutting a 1.5-cm segment each day over a period of 5 days from the same specimen at approximately the same time each day and submitting each segment to the same cryo-imaging preparation steps. The unused specimen was stored in a sealed container at 4°C. When the segments were cryo-imaged, there was a dramatic change in the appearance of the media for segments that were delayed in processing. The media appeared much redder on bright-field cryo-images and gave reduced fluorescence. This translated to a purple appearance of the media from its normal pink on pseudo-colour cryo-images (media on right side affected in Fig. 3c). The typically blue adventitia on pseudo-colour cryo-images turns green, which happens to be the same colour as diffuse haemorrhage (Fig. 3w and c). We hypothesized that a delay in processing causes haemoglobin to be released from ruptured erythrocytes in the media and adventitia. The leaked haemoglobin apparently perfuses the tissue sample and alters the appearance of the cryo-images. To effectively use cryo-imaging, we concluded that specimens should be processed within 45 h. For optimal cryo-imaging results, specimens should be embedded and stored at −80°C as soon as possible after death.

In some applications, it may be advantageous to use cryo-imaging instead of histology. Histology is labour intensive and requires experienced technicians. Tissue type identification with cryo-imaging can be done much faster. Cryo-imaging processing time from a relatively large fresh specimen (4 cm) to 3D volume rendering takes approximately 5.5 h: 1.5 h for preparation and 4 h for slicing axially the 4-cm vessel segment with 40-μm sections (~1000 sections, ~15 sec per section). This is to be compared to only a few sections every few centimetres for standard stains. Some specific histological stains require difficult and relatively long processing, especially if the whole specimen needs to be fixed and decalcified. Using histology, some tissue types are altered from their natural appearance by processing or they are not seen at all in histology. For example, unless specific lipid stains are used, lipids are washed out by standard histology processing leaving only the supporting mature collagen matrix (Fig. 3a and d). Non-fluorescent and fluorescent fibrosis are observed as dense mature collagen in histology and hence lose their fluorescence properties (Fig. 3n, p, r and t). The different types of haemorrhages are washed out and not seen in histology at all (Fig. 3k and l). Most notably, cryo-imaging does not cause tissue warping, tearing, folding or other artefacts that are often present with histology; the natural shape and appearance of the tissue is very well preserved.

Accurate high-resolution 3D volume renderings of the original vessel were created by entering the cryo-imaging data into Amira 4.1.2 visualization software (Mercury Computer Systems, Chelmsford, MA, U.S.A.). An area of active research by our lab is to determine if these renderings can be used to validate 3D imaging modalities. Figure 5 shows a sample rendering from a specimen that was not part of the validation study.

Cryo-imaging has other potential applications. Tissue types of interest can be segmented and rendered so that their distribution throughout the plaque can be studied. Special immunostains for specific proteins or cells such as metalloproteinases, macrophages, and T lymphocytes can be highlighted in Amira to show plaque distribution and quantity. Different views can be generated from the 3D renderings. Figure 5 shows how the thickness of the lipid core and fibrous cap varies significantly along the length of the vessel, which would not be apparent with histology. In conclusion, cryo-imaging offers superior visualization and identification ability than previously available.

Acknowledgements

The authors thank the Department of Pathology, University Hospitals of Cleveland for supplying the specimens.

Sources of Funding:

This work was supported by NIH grants R41HL084822 and T35 HL082544.

References

de Weert TT, Ouhlous M, Meijering E, Zondervan PE, Hendriks JM, van Sambeek MR, Dippel DW, van der Lugt A. In vivo characterization and quantification of atherosclerotic carotid plaque components with multidetector computed tomography and histopathological correlation. Arterioscler. Thromb. Vasc. Biol 2006;26:2366–2372. [PubMed: 16902158]

Doherty TM, Fitzpatrick LA, Inoue D, et al. Molecular, endocrine, and genetic mechanisms of arterial calcification. Endocr. Rev 2004;25:629–672. [PubMed: 15294885]

Fleiner M, Kummer M, Mirlacher M, Sauter G, Cathomas G, Krapf R, Biedermann BC. Arterial neovascularization and inflammation in vulnerable patients: early and late signs of symptomatic atherosclerosis. Circulation 2004;110:2843–2850. [PubMed: 15505090]

Granada JF, Wallace-Bradley D, Win HK, et al. In vivo plaque characterization using intravascular ultrasound-virtual histology in a porcine model of complex coronary lesions. Arterioscler. Thromb. Vasc. Biol 2007;27:387–393. [PubMed: 17138936]

Larose E, Yeghiazarians Y, Libby P, et al. Characterization of human atherosclerotic plaques by intravascular magnetic resonance imaging. Circulation 2005;112:2324–2331. [PubMed: 16203910]

Libby P, Ridker PM, Maseri A. Inflammation and atherosclerosis. Circulation 2002;105:1135–1143. [PubMed: 11877368]

Lovett JK, Redgrave JN, Rothwell PM. A critical appraisal of the performance, reporting, and interpretation of studies comparing carotid plaque imaging with histology. Stroke 2005;36:1091–1097. [PubMed: 15774817]

Prentice AI. Autofluorescence of bone tissues. J. Clin. Pathol 1967;20:717–719. [PubMed: 5602982]

Ross R. Atherosclerosis–aninflammatory disease. N. Engl. J. Med 1999;340:115–126. [PubMed: 9887164]

Salvado, O.; Hoffman, R.; Yutzy, S.; Roy, D.; Wilson, DL. 3D voxel based validation of MR vascular imaging using cryoimaging. MICCAI: 1st International Workshop on Computer Vision for Intravascular and Cardiac Imaging; Copenhagen, Denmark. 2006a. p. 98-105.2006

Salvado, O.; Roy, D.; Heinzel, M.; McKinley, E.; Wilson, DL. 3D Cryo-section/imaging of blood vessel lesions for validation of MRI data. International Society for Optical Engineering volume 6142 of Physics of Medical Imaging; March 2006; San Diego, CA, USA. SPIE; 2006b.

Stary HC, Chandler AB, Glagov S, et al. A definition of initial, fatty streak, and intermediate lesions of atherosclerosis. A report from the Committee on Vascular Lesions of the Council on Arteriosclerosis, American Heart Association. Arterioscler. Thromb. Vasc. Biol 1994;14:840–856.

Stary HC, Chandler AB, Dinsmore RE, et al. A definition of advanced types of atherosclerotic lesions and a histological classification of atherosclerosis. A report from the Committee on Vascular Lesions of the Council on Arteriosclerosis, American Heart Association. Circulation 1995;92:1355–1374. [PubMed: 7648691]

Yuan C, Kerwin WS, Yarnykh VL, et al. MRI of atherosclerosis in clinical trials. NMR Biomed 2006;19:636–654. [PubMed: 16986119]

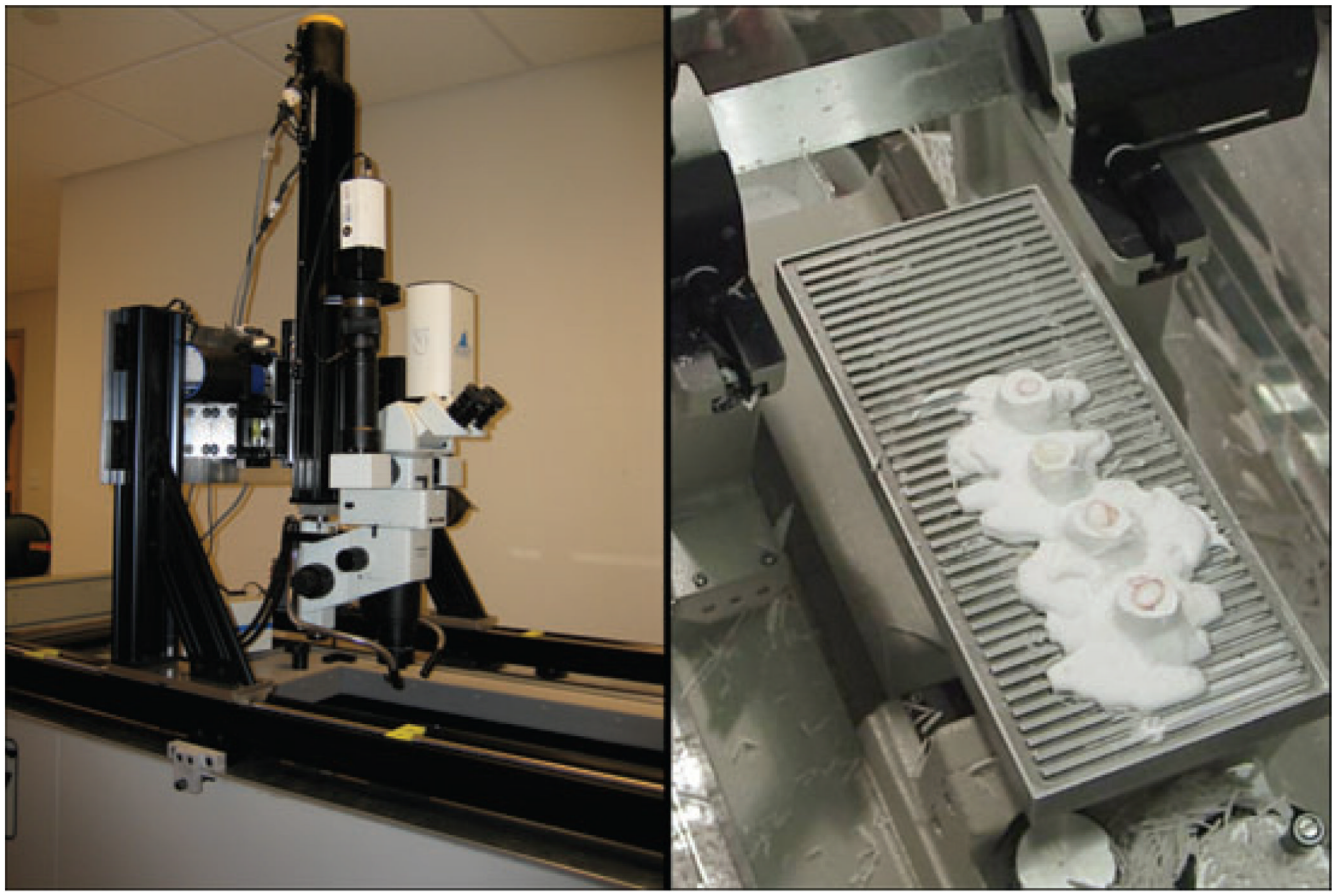

Fig. 1.
Cryo-imaging apparatus. Block face images of embedded frozen tissue samples are captured with an episcopic microscope and CCD camera and processed using image processing techniques.

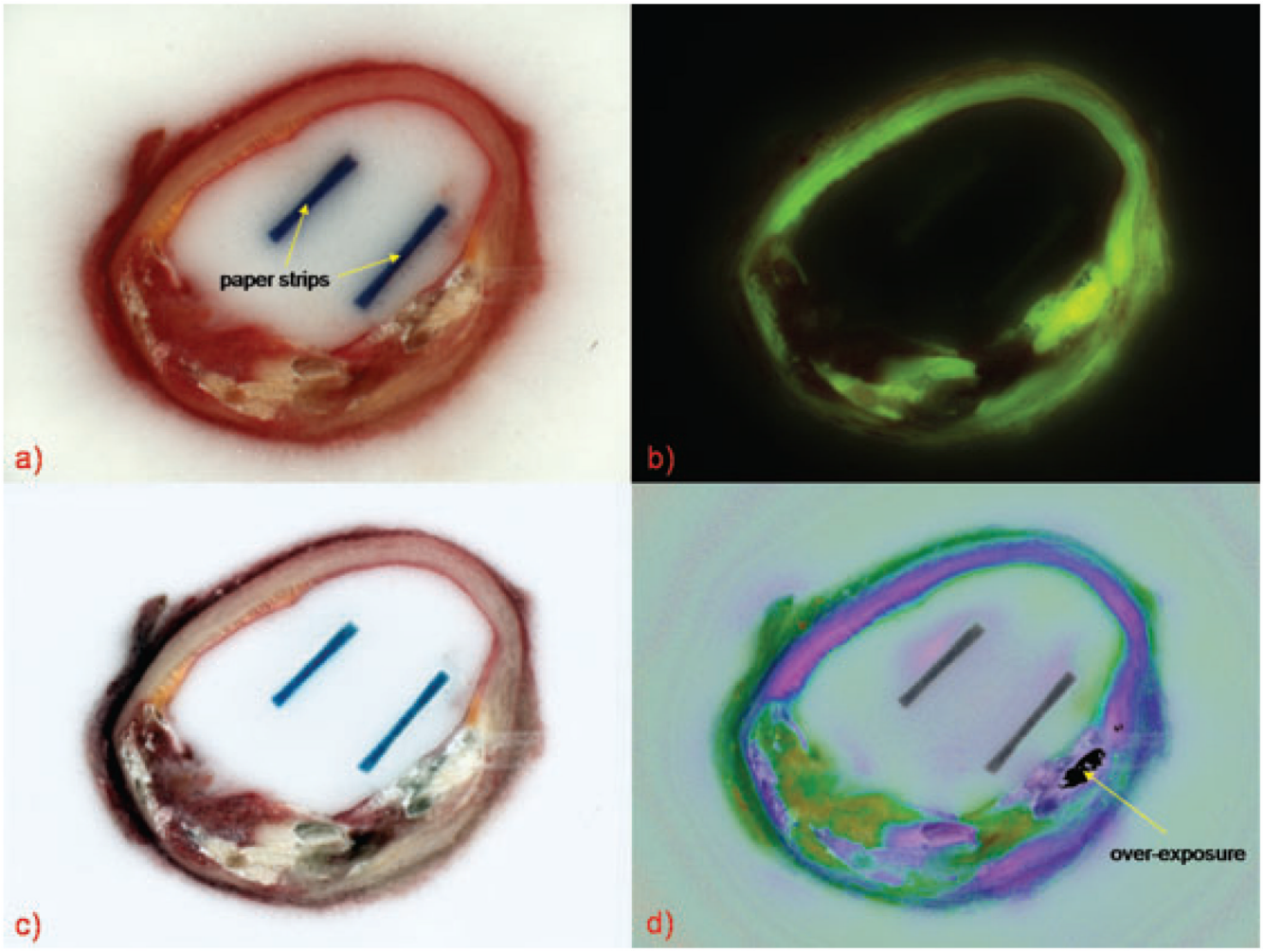

Fig. 2.
(a) bright-field, (b) fluorescence, (c) contrast-enhanced and (d) pseudo-colour cryo-images of the same block face. Paper strips used to keep the sample upright during freezing appear as two dark rectangular areas and do not interfere with interpretation of cryo-images. The region of overexposure is from the fluorescence image.

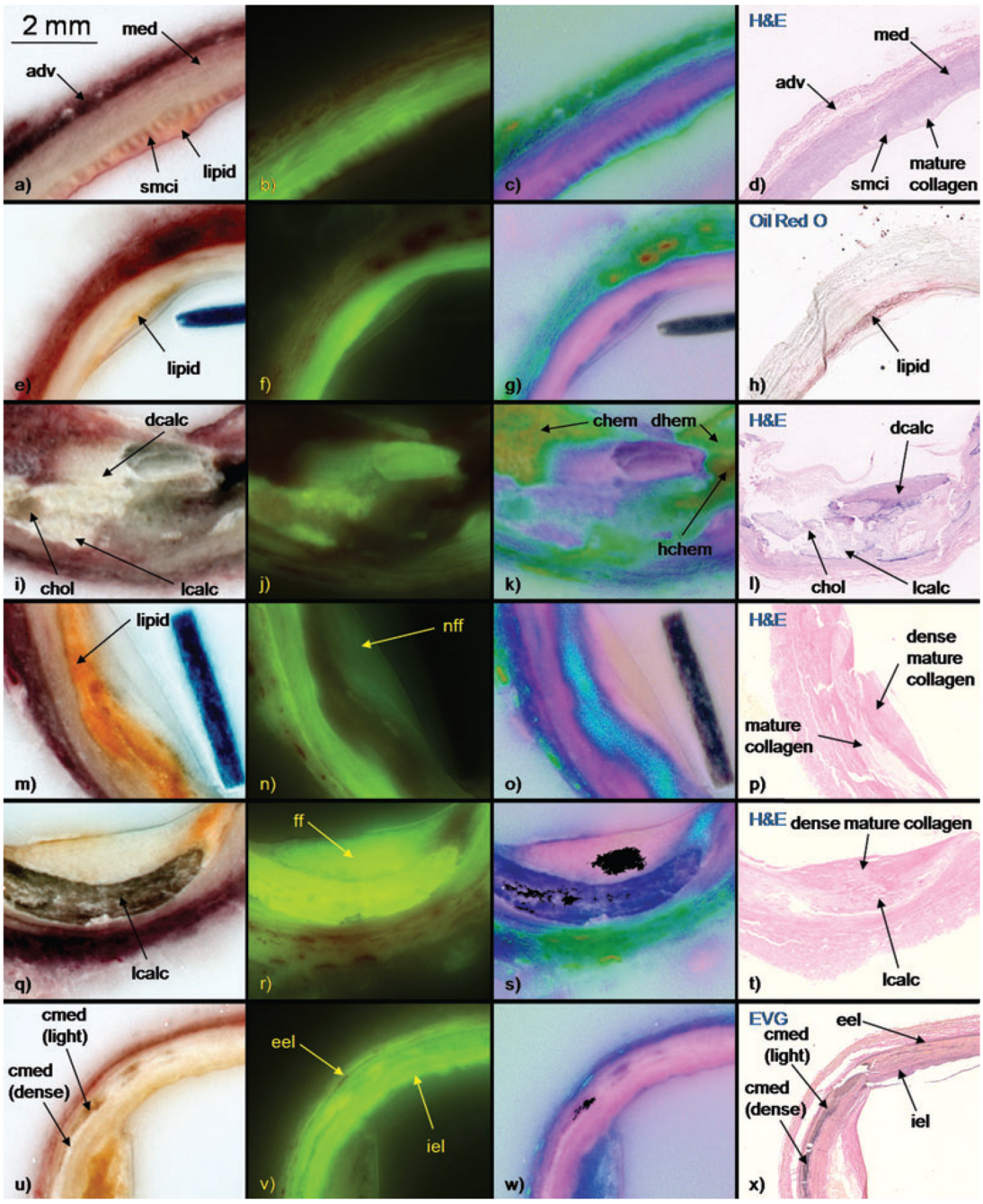

Fig. 3.

Examples of each tissue type in contrast-enhanced bright-field, fluorescence, and pseudo-colour cryo-images and corresponding histology (haematoxylin and eosin, Elastic van Gieson, Mallory's trichrome and Oil Red O). The stain is shown in upper left corner of each histology panel. Images from each row are from same block face.

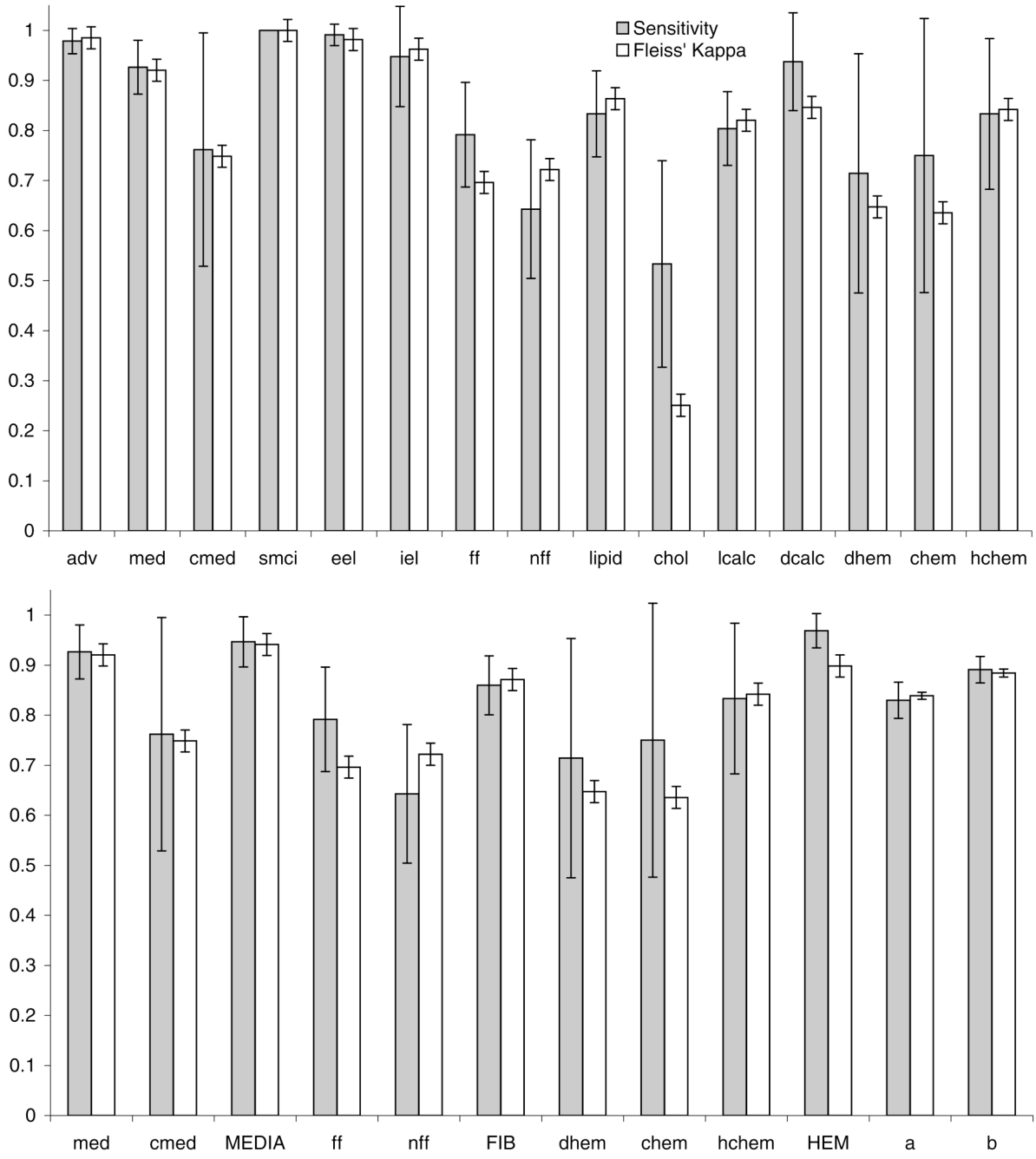

Fig. 4.

(a) Graphs of sensitivity and Fleiss' Kappa for all tissue type categories with 95% confidence intervals. (b) Graphs showing media, fibrosis and haemorrhage combined categories and totals for all tissue types with and without combined categories.

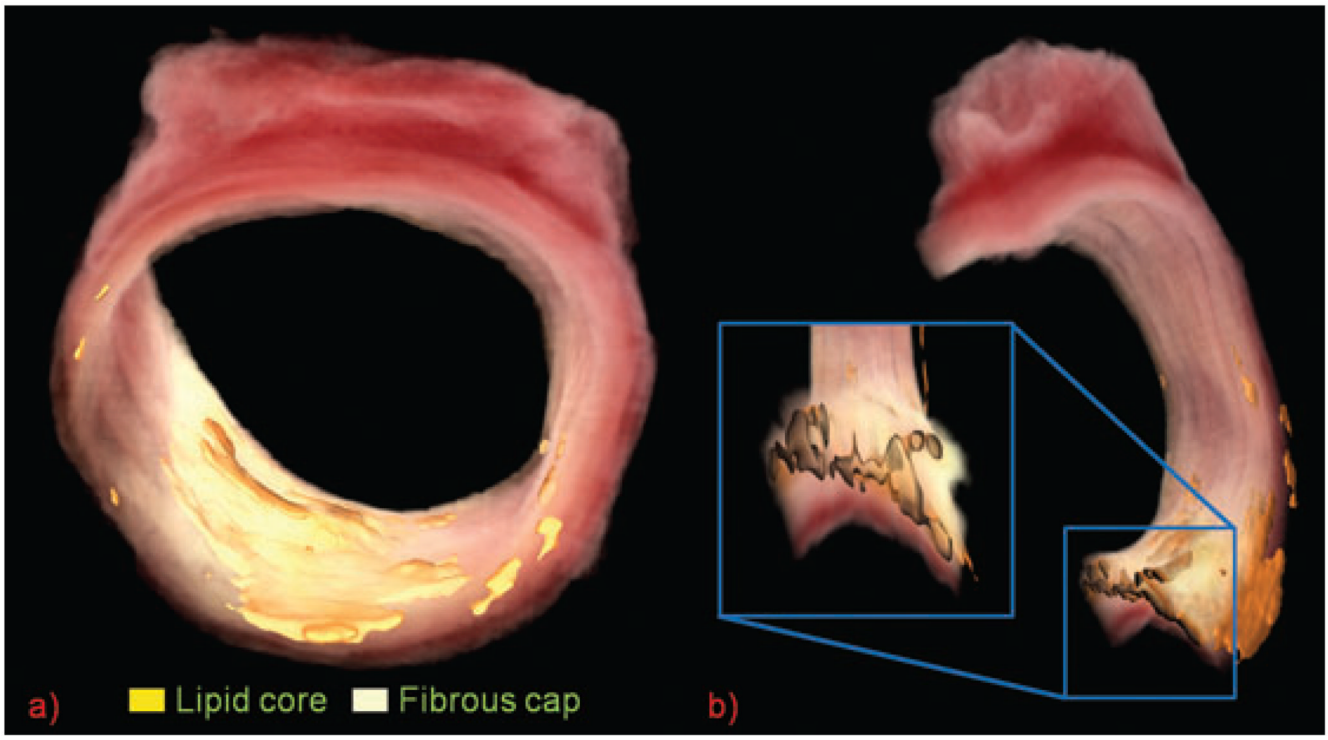

Fig. 5.
(a) 3D volume rendering of bright-field cryo-images sliced every 40 μm. Lipid regions are highlighted with surface rendering. The hazy white fibrous cap covers the lipid areas. (b) Cut view of same vessel. Variability in the thickness of the lipid core and fibrous cap is seen in inset.

Table 1

Tissue type characteristics table. These tissue types were identified on bright-field, fluorescence and pseudo-colour cryo-images and validated with histology (haematoxylin and eosin, Elastic van Gieson, Mallory's trichrome and Oil Red O). The fluorescence scale ranges from 0/+ to ++++. Tissue type abbreviations used in figures are shown in brackets.

Tissue type	Bright field	Fluorescence	Pseudo-colour	Histology
Adventitia [adv]	Red	++	Blue – normal Green – blood saturated	
Media [med]	Pink – normal Red – blood saturated	+++	Pink – normal Purple – blood saturated	
Calcification in media [cmed]	Yellow-brown – light Chalky white – dense	++++ – light 0/+ – dense	Dark purple/blue – light Purple/pink – dense	Patchy light or dense calcification in media
Smooth muscle cell ingrowth [smci]	Pink (fingerlike)	+++	Pink	Smooth muscle cell extending beyond internal elastic lamina into intima
External elastic lamina [eel]	Not discernable	++++	Not discernable	Easily seen on EVG stain
Internal elastic lamina [iel]	Not discernable	++++	Not discernable	Easily seen on EVG stain
Fluorescent fibrosis [ff]	White	+++	Light pink	Dense mature collagen
Non-fluorescent fibrosis [nff]	White	0/+	Light pink	Dense mature collagen
Lipid	Yellow/orange	0/+	Blue/turquoise	Mature collagen
Cholesterol clefts [chol]	Yellow-brown	++	Blue-green	
Light calcification [lcalc]	Chalky white/ yellow-brown	++++	Dark purple/blue	Lighter, speckled staining calcification
Dense calcification [dcalc]	Chalky white	++++	Light purple/pink	Darker staining calcification
Diffuse haemorrhage [dhem]	Red	0/+	Green	Washed out by processing and not observed in histology
Concentrated haemorrhage [chem]	Red	0/+	Yellow	Washed out by processing and not observed in histology
Highly concentrated haemorrhage [hchem]	Red	0/+	Red	Washed out by processing and not observed in histology

Table 2

Contingency table of results for all raters for all tissue types. Perfect agreement would give all values in the diagonal and zeros everywhere else.

	Histology ground truth														
Rater results	**adv**	**med**	**cmed**	**smci**	**eel**	**iel**	**Ff**	**nff**	**lipid**	**chol**	**lcalc**	**dcalc**	**dhem**	**chem**	**hchem**
Adv	229	1	0	0	0	0	0	0	0	0	0	0	0	0	0
med	0	239	5	0	0	6	4	2	0	0	0	0	0	0	0
cmed	0	8	32	0	0	0	0	0	2	0	0	0	0	0	0
smci	0	0	0	18	0	0	0	0	0	0	0	0	0	0	0
eel	1	0	0	0	113	2	0	0	0	0	0	0	0	0	0
iel	0	0	0	0	1	182	1	0	0	0	0	0	0	0	0
ff	0	4	30	0	0	1	133	50	6	0	1	2	0	0	0
nff	0	1	1	0	0	0	7	135	3	0	0	2	0	0	0
lipid	0	0	0	0	0	0	4	10	295	1	1	0	0	0	0
chol	0	0	0	0	0	0	0	8	37	16	21	2	3	0	0
lcalc	0	5	0	0	0	1	7	3	4	1	164	3	0	0	0
dalc	0	0	1	0	0	0	12	2	5	1	17	135	0	0	0
dhem	2	0	0	0	0	0	0	0	2	11	0	0	30	3	0
chem	2	0	0	0	0	0	0	0	0	0	0	0	8	18	5
hchem	0	0	0	0	0	0	0	0	0	0	0	0	1	3	25

Table 3

Contingency table of results of all raters when certain tissue type categories are combined. MEDIA, FIB and HEM are combinations of med and cmed, ff and nff, and dhem, chem. and hchem, respectively. A cleaner diagonal is apparent with combined categories.

	Histology ground truth										
Rater Results	**adv**	**MEDIA**	**smci**	**eel**	**iel**	**FIB**	**lipid**	**chol**	**lcalc**	**dcalc**	**HEM**
adv	229	1	0	0	0	0	0	0	0	0	0
MEDIA	0	284	0	0	6	6	2	0	0	0	0
smci	0	0	18	0	0	0	0	0	0	0	0
eel	1	0	0	113	2	0	0	0	0	0	0
iel	0	0	0	1	182	1	0	0	0	0	0
FIB	0	9	0	0	1	325	9	0	1	4	0
lipid	0	0	0	0	0	14	295	1	1	0	0
chol	0	0	0	0	0	8	37	16	21	2	3
lcalc	0	5	0	0	1	10	4	1	164	3	0
dcalc	0	1	0	0	0	14	5	1	17	135	0
HEM	4	0	0	0	0	0	2	11	0	0	93